

Article

Effect of Substrate Temperature on the Optical and Electrical Properties of Nitrogen-Doped NiO Thin Films

Yuan Tian ^{1,2,*}, Lianguo Gong ^{1,2}, Xueqian Qi ³, Yibiao Yang ^{1,2,*} and Xiaodan Zhao ^{1,2}

¹ Key Lab of Advanced Transducers and Intelligent Control System, Ministry of Education and Shanxi Province, Taiyuan University of Technology, Taiyuan 030024, China

² College of Physics and Optoelectronics, Taiyuan University of Technology, Taiyuan 030024, China

³ First Design and Research Institute, China Wuzhou Engineering Group Corporation LTD, Beijing 100053, China

* Correspondence: tianyuan01@tyut.edu.cn (Y.T.); yangyibiao@tyut.edu.cn (Y.Y.)

Received: 21 August 2019; Accepted: 26 September 2019; Published: 2 October 2019



Abstract: NiO is a widely used p-type semiconductor. The desired optical and electrical properties of NiO vary in different application fields. To modulate the properties of NiO, nitrogen (N)-doped NiO thin films were synthesized by reactive radio-frequency magnetron sputtering on ITO-coated glass substrates. The influence of substrate temperature on the properties of NiO was investigated. XRD studies indicated a cubic structure. With the increase of the substrate temperature, the average transmittance in the visible region gradually reduced from 90% to 50%. The bandgap energy narrowed from 3.5 to 3.08 eV. The intensity of the PL spectra weakened, and the electrical conductivity rose. Overall, changing the substrate temperature is an effective method to modulate the optical and electrical properties of N-doped NiO thin films.

Keywords: nitrogen-doped; nickel oxide; magnetron sputtering; substrate temperature; optical properties; electrical properties

1. Introduction

As a promising metal-oxide material in the semiconductor field, NiO has attracted a lot of attention in recent years. NiO is a wide-bandgap p-type semiconductor applied as a transparent conducting film [1], electrode in electrochromic devices [2], and functional layer for chemical sensors [3]. These applications strongly depend on its optical and electrical properties. Therefore, it is crucial to modulate the optical and electrical properties of NiO thin films to exploit its applications. There are many methods to fabricate NiO thin films, such as chemical vapor deposition [4], facile sol-gel synthesis [5], magnetron sputtering [6], spray pyrolysis [7], and pulsed laser deposition [8]. Among them, magnetron sputtering is the most used, with the advantages of high quality, good adhesion, low growth temperature, and high efficiency [9]. In general, changing the deposition conditions, heating treatment, and doping is effective to regulate the optical and electrical properties of NiO thin films. Many studies report the variation of NiO thin films' properties with the deposition conditions. Nandy et al. [10] studied the effect of oxygen partial pressure on the electrical and optical properties of NiO thin films. The electrical conductivity and transparency decreased with increasing oxygen partial pressure. Meanwhile, the bandgap narrowed. Sato [11] observed a gradual increase of resistivity with the increasing of substrate temperature. The influence of the heating treatment was studied as well. The resistivity increased with heating, while the transparency increased gradually from 40% to 80% as the temperature increased from 100 to 400 °C and then decreased to 60% when the temperature reached 500 °C. Considering the small adjustments possible for deposition conditions and heating treatment to modulate NiO

properties, doping was identified as the most effective approach. Al-doped NiO showed enhanced electrical conductivity [12]. On the contrary, Li-doped NiO displayed significantly decreased electrical conductivity. In 2017, Keraudy [13] deposited N-doped NiO thin films on a Ni metal target by mixing reactive N₂ and O₂ to non-reactive Argon. The influence of the N/O rate on the optical and electrical properties was studied. However, as the O content has a strong impact on the properties of NiO thin films, the result obtained actually was due to the synergistic effects of N doping and the change of O content. In this paper, N-doped NiO thin films were grown on a NiO ceramic target by mixing N₂ to Argon. To modulate the properties of the N-doped NiO thin film, the evolution of the optical and electrical properties with substrate temperature was investigated.

2. Materials and Methods

NiO thin films were deposited by reactive radio-frequency magnetron sputtering onto commercially purchased ITO (sheet resistance value: 20 Ω/cm, size: 2 cm × 2 cm)-coated glass substrates. The substrates were cleaned with soapy water, alcohol, and deionized water successively. A NiO ceramic target (99.99% purity) of 6 cm in diameter and 3 mm in thickness was used. The base pressure was 2×10^{-5} Pa, and the working pressure was 1 Pa. The sputter power was kept at 60 W. The distance between target and substrate was 5 cm and remained constant throughout the sputtering process. An undoped NiO thin film was deposited using Ar at room temperature. N-doped NiO thin films were deposited in the presence of 20% Ar/80% N₂, at different substrate temperatures, i.e., room temperature, 100, 200, 300 and 400 °C. The thickness of the films was 300 nm, detected by an INFICON STM-2XM thickness monitor (Bad Ragaz, Switzerland).

The surface morphologies of the resulting films were observed by field emission scanning electron microscopy (FE-SEM: Hitachi S4800) and atomic force microscopy (AFM: NT-MDT Prima, Moscow, Russia). An X-ray diffractometer (Philips X'pert PRO, Amsterdam, Netherlands) equipped with Cu K α radiation was adopted to analyze the structure. Room-temperature Raman spectroscopy was carried out by a Renishaw Raman spectrometer using a 532 nm solid-state laser as the excitation source. X-ray photoelectron spectroscopy (XPS) measurements were performed by Thermo ESCALAB 250XI (Waltham, MA, USA) with Al K α radiation. UV-Vis transmittance spectra were obtained by a spectrofluorometer (FS5-Edinburgh Instruments, Livingston, UK). Room-temperature photoluminescence (PL) was performed with a 325 nm He-Cd laser as the excitation source. The Mott-Schottky plots were obtained in a three-electrode glass cell using a 0.5 M Na₂SO₄ aqueous solution connected to an electrochemical workstation (CHI760E, Beijing Huake Putian technology limited liability company, Beijing, China). A platinum electrode and an Ag/AgCl electrode were selected to be the counter electrode and the reference electrode, respectively. The impedance of NiO thin films was measured in an electrochemical workstation. The two electrodes were connected with the impedance measuring system, as shown in Figure 1. During measurement, a = 1 cm, b = 2 cm.

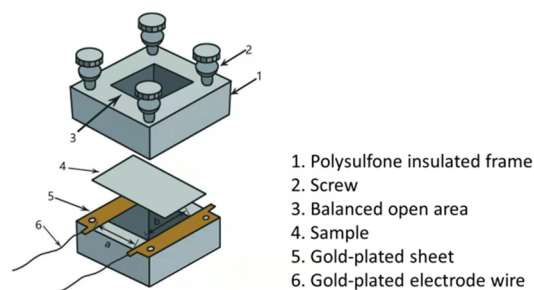


Figure 1. Impedance measuring system.

3. Results

Table 1 reports the deposition rate as a function of the substrate temperature. The deposition rate slightly increased with the substrate temperature. Although the target was cooled by running water,

the temperature of the target surface increased as the substrate temperature increased, which resulted in an increase of the activation energy of atoms and then an increase of the sputtering rate.

Table 1. Deposition rate at different substrate temperature.

Substrate Temperature (°C)	Deposition Rate (nm/min)
RT	82
100 °C	83
200 °C	85
300 °C	88
400 °C	94

Figure 2 shows the surface morphologies of ITO, undoped NiO, and N-doped NiO thin films deposited at different substrate temperatures. All NiO samples were poly-crystalline films with grain-subgrain structure, owing to the impact of the grain-subgrain structure of ITO (Figure 2a). Grains were distributed into highly oriented regions. Region A was composed of squares subgrains, while region B consisted of bar-type subgrains. Compared with undoped NiO films (Figure 2b), N-doped NiO films (Figure 2c) were looser, owing to the negative effect of N₂ on film quality during magnetron sputtering. According to Figure 2c–g, with the increase of substrate temperature, region A shrank and region B increases. Meanwhile, the subgrains became sags and crests. By changing the focus of SEM, it was revealed that the thickness of region A was greater than that of region B.

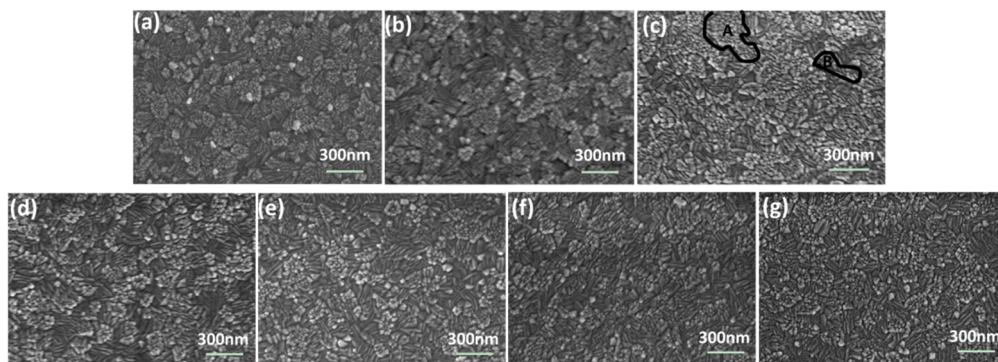


Figure 2. Surface SEM images of (a) ITO, (b) undoped NiO films at room temperature, and (c) N-doped NiO thin films at room temperature, (d) 100 °C, (e) 200 °C, (f) 300 °C, (g) 400 °C.

To determine the thickness difference between region A and region B of NiO thin films, AFM measurements were performed. Figure 3a shows an AFM surface image ($1 \times 1 \mu\text{m}^2$ scan area) of an N-doped NiO thin film at room temperature. Figure 3b illustrates the thickness variation along the line in Figure 3a. According to Figure 3b, region A was 9 nm thicker than region B, on average.

Figure 4a shows the XRD spectra of NiO thin films at different substrate temperatures. The XRD spectra indicated a cubic NiO phase. However, according to the literature, at temperatures above the Néel temperature (523 K), the crystal structure of NiO is cubic, whereas below the Néel temperature, the crystals become slightly distorted from this cubic structure and acquire a rhombohedral structure which accompanies the antiferromagnetic ordering [14,15]. The difference between the angles of the rhombohedral and the fcc NiO was very small, due to the broadening of the peaks, and no difference appeared in the XRD spectra. The diffraction peaks around 37.2° and 41.2° were assigned to NiO (111) and NiO (200), while the others are characteristic of the ITO layers [16]. Diffraction peaks of (220) at 62.9° and (311) at 75.4° were not visible, which indicated a preferred orientation of the NiO thin films. As seen in Figure 4b, the (111) peak position of undoped and N-doped NiO thin films is the same. The (111) peak shifted towards a higher angle as the temperature increased from room temperature to 400 °C, corresponding to a smaller interplanar spacing, as shown in Figure 4c.

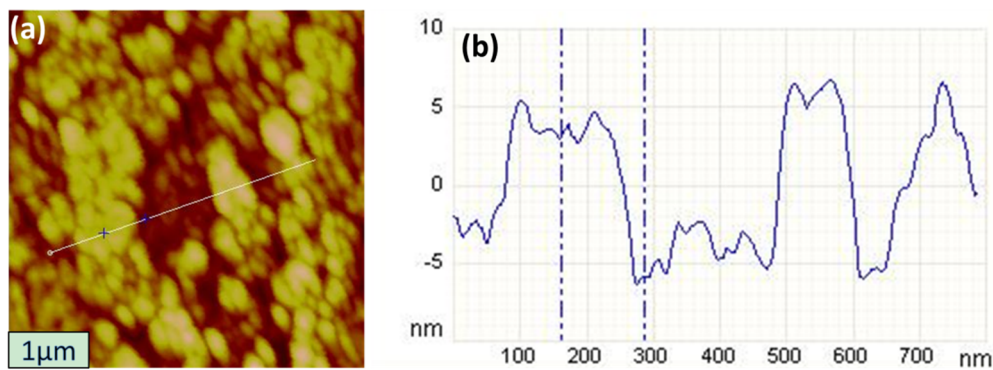


Figure 3. (a) AFM images of N-doped NiO thin films at room temperature and (b) thickness profile along the line in (a) across region A and region B.

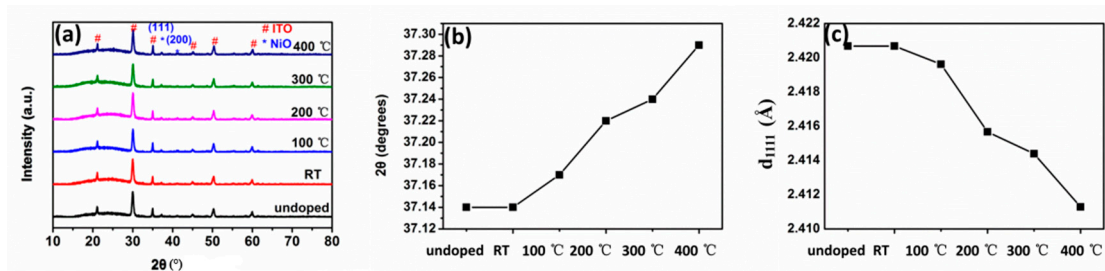


Figure 4. (a) XRD spectra of NiO thin films at different substrate temperatures and evolution of (b) angular position and (c) interplanar spacing of (111).

The room-temperature Raman scattering spectra of NiO thin films at different substrate temperatures are shown in Figure 5. Four peaks were observed. Raman peaks located at about 458 and 599 cm^{-1} corresponded to the transverse optical (TO) and longitudinal optical (LO) phonon modes of NiO, respectively. It was suggested that the appearance of LO phonon may be due to Ni vacancy defects [17–19]. Two other peaks, at 783 and 1100 cm^{-1} , were assigned to two-phonon scattering 2TO and 2LO, respectively. These results further proved the crystalline structure of NiO.

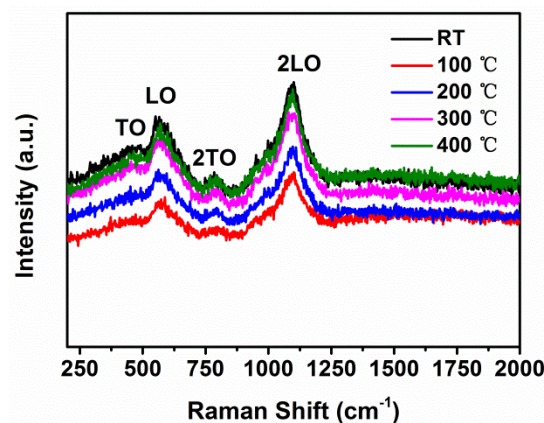


Figure 5. Raman scattering spectra of NiO thin films at different substrate temperatures.

The surface elemental composition and state of NiO thin films were analyzed by XPS, as shown in Figure 6. The XPS survey spectra in Figure 6a show the peaks characteristics of nickel, oxygen, nitrogen, and carbon in all samples. The Ni 2p spectra (Figure 6b) contained six components. The peaks at 853.9 and 872.8 eV were attributed to Ni²⁺, and the peak at around 861.1 eV is their satellite (sat.) peak. The peak at 855.7 eV was assigned to Ni³⁺ [20]. A shakeup-type satellite peak of Ni 2p_{1/2} was detected at 879.7 eV. The O 1s spectra shown in Figure 6c contain two peaks at 529.6 and 531.4 eV,

corresponding to Ni–O and Ni₂O₃ [21]. N 1s spectra are shown in Figure 6d. The peaks located at 396.7 and 397.8 eV were assigned to atomic N in Ni oxide lattice [22] and N atom bonded to O [23], respectively. The other two peaks at 400.2 and 402.0 eV could be attributed to nitrogen atoms related to N–O bonds due to surface oxidation and ammonium-type bonds [24–26].

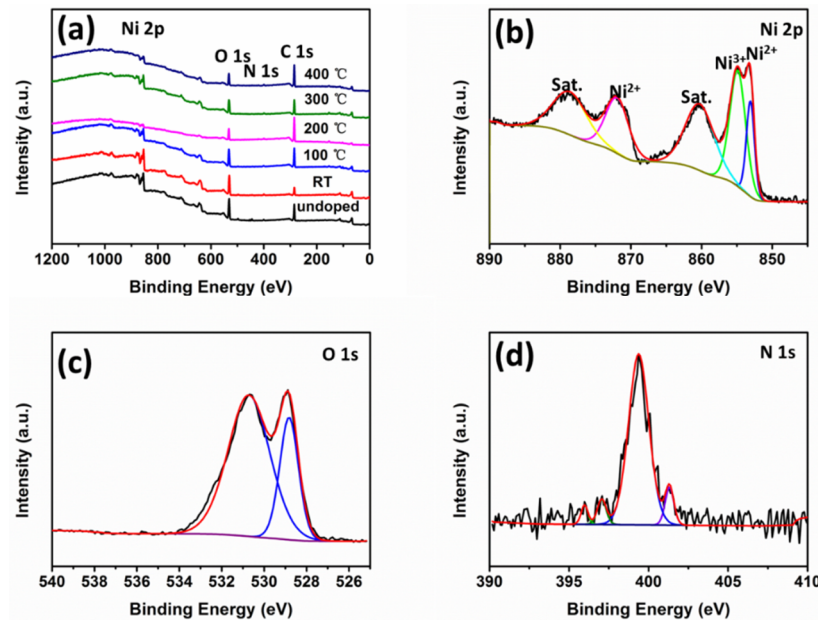


Figure 6. (a) XPS survey spectra of NiO films deposited at different substrate temperatures and (b) Ni 2p spectra, (c) O 1s spectra, (d) N 1s spectra of N-doped NiO thin films at room temperature.

The N 1s spectra of NiO films deposited at different substrate temperatures are shown in Figure 7a. For undoped NiO films, the absence of peaks located at 396.7 and 397.8 eV indicated that no N was incorporated into NiO films. The peaks at 396.7 and 397.8 eV appeared when N₂ was adopted as the reactive gas. However, these two peaks were very weak at room temperature, corresponding to the small content of N in NiO. As the substrate temperature increased, the peaks at 396.7 and 397.8 eV became obvious, and the area of these two peaks increased. According to Figure 7a, the N content in NiO films increased with the substrate temperature. The content of N on the surface of NiO films obtained from XPS is shown in Figure 7b. For undoped NiO films, N concentration was 2.17%, owing to surface N absorption. When N₂ was adopted as the reactive gas, the N concentration increased slightly to 2.52%. With the substrate temperature increasing to 100, 200, 300 and 400 °C, N concentration on the surface of NiO increased to 2.71%, 3.34%, 3.39% and 4.20%.

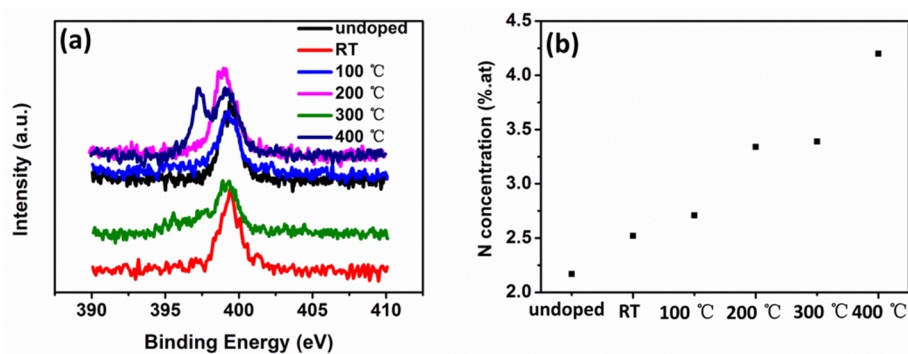


Figure 7. (a) N 1s spectra of NiO thin films and (b) N content as a function of substrate temperature.

The color of N-doped NiO thin films transformed from semitransparent grey to opaque dark brown as the substrate temperature varied from room temperature to 400 °C. Ni³⁺ is responsible to the

coloring of NiO [27]. In fact, the incorporation of N in NiO is an endothermic reaction [28] ($\Delta H_f > 0$). This positive heat of formation indicates that N doping requires a net energy input. Heating provides external energy and promotes N doping. Thus, as the substrate temperature rises, the N content of the NiO thin films increased, and Ni^{3+} increased correspondingly.

UV-Vis transmittance spectra of NiO thin films are shown in Figure 8. The effect of the ITO layer and glass on the transmittance was deducted as baseline. The transmittance of NiO thin films at room temperature reduced slightly when N was doped. For N-doped NiO, the average transmittance in the visible region reduced from 90% to 50% gradually as the temperature increased from room temperature to 400 °C. The reduced transmittance was associated with the increase of Ni^{3+} [27]. The optical bandgap energy (E_g) of N-doped NiO thin films at different substrate temperatures is shown in Figure 4b. It was determined from the Tauc's plot shown in the inset. The Tauc's plot was calculated using the Tauc's relation below:

$$\alpha h\nu = B(h\nu - E_g)^{1/2} \quad (1)$$

where $h\nu$ is the photon energy, B is a constant, E_g is the optical bandgap energy, and α is the absorption coefficient given by the relation:

$$I = I_0 \exp(-\alpha t) \quad (2)$$

where t is the film thickness, I is the transmitted intensity at a particular wavelength, and I_0 is the incident intensity.

The optical bandgap energy of the films was evaluated by extrapolating the linear region to zero absorption coefficient from the Tauc plots. The bandgap energy value for undoped NiO thin films was 3.53 eV. The bandgap energy values for N-doped NiO thin films at room temperature, 100, 200, 300 and 400 °C were 3.5, 3.45, 3.38, 3.33 and 3.08 eV, respectively. According to reference [29], N-doping leads to bandgap narrowing. As N concentration increased with the temperature, the bandgap energy of N-doped NiO thin films decreased.

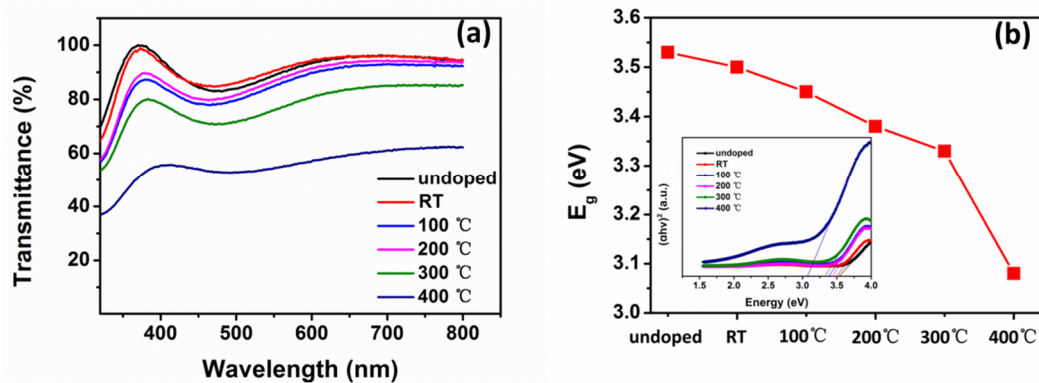


Figure 8. (a) UV-Vis transmittance spectra and (b) optical bandgap energy of NiO thin films deposited at different substrate temperatures.

Mott-Schottky plots of NiO thin films (Figure 9a) were adopted to assess the valence band edge potential (E_{VB}). Since the valence band edge potential practically coincides with the flat band potential for p-type semiconductors, the Mott-Schottky relation can be used as follows [30]:

$$\frac{1}{C^2} = -\frac{2}{\epsilon\epsilon_0 e N_A} \left(E - E_{FB} - \frac{kT}{e} \right) \quad (3)$$

where ϵ is the permittivity of the samples, ϵ_0 is the permittivity of free space, e is the elementary charge, N_A is the donor density, E is the applied potential, E_{FB} is the flat band potential, k is the Boltzmann's constant, T is the temperature of operation, and C is the space charge capacitance. The space charge capacitance was determined by measuring the electrochemical impedance. An AC-voltage signal with

amplitude of 0.01 V was applied at 1000 Hz. The capacitance was calculated from the imaginary part of the measured impedance Z_{imag} [30]:

$$C = \frac{1}{2\pi f Z_{\text{imag}}} \quad (4)$$

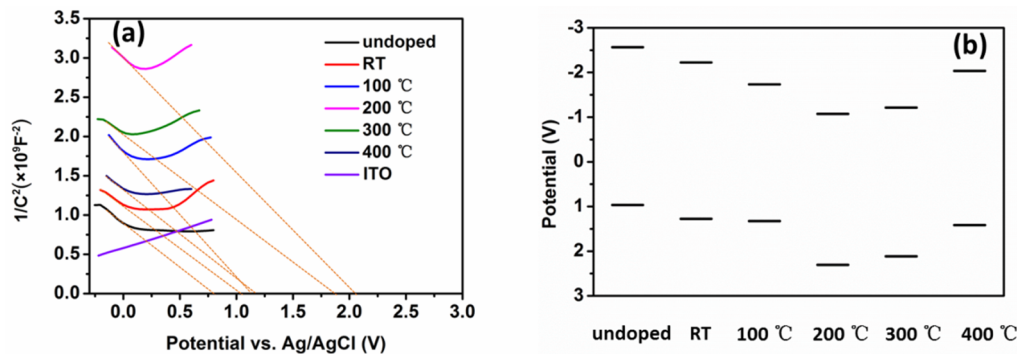


Figure 9. (a) Mott–Schottky plots and (b) schematic energy band diagrams of NiO thin films deposited at different substrate temperatures.

The Mott–Schottky plots were constructed as a function of the applied DC potential. The Mott–Schottky plots of all samples were obtained using an Ag/AgCl electrode in 1 M NaSO₄ aqueous solution. The Mott–Schottky plots showed a V shape curve revealing a p–n junction structure of ITO layer and NiO thin film. The Mott–Schottky plot of the ITO layer in Figure 9a exhibits a positive slope, confirming an n-type conductivity. According to Figure 9a, all N-doped NiO thin films were p-type semiconductors. The flat band potential E_{FB} is the intercept of the plot linear part with the potential axis. The E_{FB} of undoped NiO thin films versus the Ag/AgCl electrode was 0.75 V. The E_{FB} of N-doped NiO thin films versus the Ag/AgCl electrode was 1.06, 1.13, 2.09, 1.9, 1.2 V as the substrate temperature increased from room temperature to 100, 200, 300 and 400 °C. E_{VB} values were calculated according to the equation [31]:

$$E_{\text{VB}} = E_{\text{FB(NHE,PH=7)}} \approx E_{\text{FB(Ag/AgCl,PH=7)}} + \Delta E \quad (5)$$

where $\Delta E = 0.21$ V is the Ag/AgCl potential against a normal hydrogen electrode (NHE).

The conduction band edge potential (E_{CB}) values were calculated according to the equation [31]:

$$E_{\text{CB}} = E_{\text{VB}} - E_{\text{g}}/e \quad (6)$$

where E_{g} is the optical band gap energy obtained from UV–Vis transmittance spectra.

The calculated energy band diagrams are shown in Figure 9b. According to Figure 9b, the potential of the bands first downshifted and then upshifted with the increase of temperature. The potential of the bands was minimum at 200 °C.

According to Figure 10, the impedance of undoped NiO thin film was 28.3 Ω. The impedance of N-doped NiO thin films decreased from 28 to 27.5, 26, 21, 16 Ω as the temperature increased from room temperature to 100, 200, 300, 400 °C. As the electrical conductivity is inversely proportional to the impedance, the electrical conductivity improved with the increase of the temperature. According to the literature, the electrical conductivity is proportional to the transfer of positive charge from cation to cation through the lattice [32], i.e., [Ni³⁺]. With the increase of the temperature, [Ni³⁺] increased, thus the electrical conductivity increased.

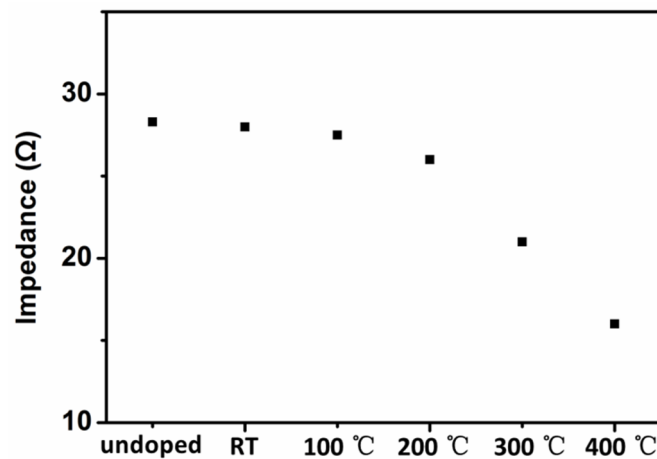


Figure 10. Impedance of samples deposited at different substrate temperatures.

Figure 11 presents the room temperature PL spectra of NiO thin films at different substrate temperatures. For all samples, a dominant near band edge (NBE) emission peak centered at 395 nm (3.14 eV) and a weak emission peak at 524 nm (2.37 eV) can be clearly seen. The NBE emission originates from the direct recombination of the excitons through exciton–exciton scattering [33]. The weak emission at 524 nm is attributed to the radiative recombination of a photo-generated hole with an electron occupying the nickel and oxygen vacancies [34]. Compared with undoped NiO thin films, it can be seen that the N-doped NiO thin films exhibited PL signals with a similar curve shape, demonstrating that N-doping did not give rise to new PL phenomena. Indeed, the dopant in a stable chemical state will not generate different PL phenomena, because it is unable to capture electrons. The PL intensity of NiO thin films decreased as the temperature rose from room temperature to 400 °C. It is thought that the difference of the emission intensity likely depends on morphology variations. [35]

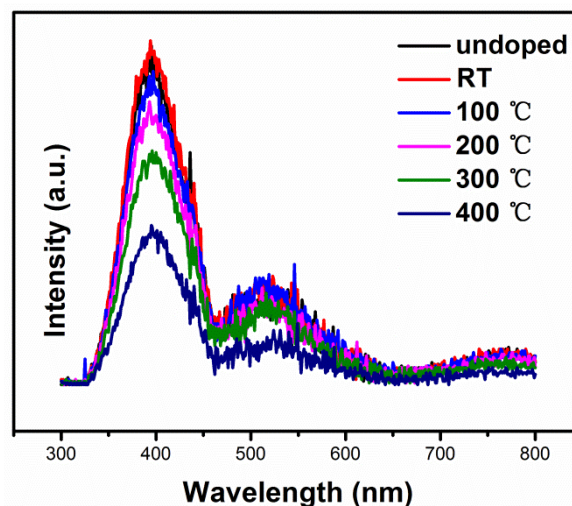


Figure 11. Room-temperature photoluminescence (PL) spectra of NiO thin films deposited at different substrate temperatures.

4. Conclusions

N-doped NiO thin films at different substrate temperatures were prepared by radio-frequency reactive magnetron sputtering. The influence of substrate temperature on the optical and electronic properties was investigated. According to the research, the transmittance of N-doped NiO decreased with the increase of the substrate temperature. The energy band structure was determined by analyzing transmittance spectra and Mott–Schottky plots. The energy band gap shrank as the substrate

temperature rose. The valence band edge potential and conduction edge potential increased when the substrate temperature increased from room temperature to 200 °C, then decreased as the substrate temperature continued to rise. The intensity of the PL spectra decreased and the conductivity increased.

Author Contributions: Conceptualization, Y.T.; Methodology, Y.T.; Software, Y.T.; Validation, Y.T., Y.Y. and X.Z.; Formal Analysis, Y.T.; Investigation, L.G.; Resources, Y.Y.; Data Curation, X.Q.; Writing—Original Draft Preparation, Y.T.; Writing—Review and Editing, Y.T.; Visualization, Y.T.; Supervision, Y.Y.; Project Administration, Y.T.; Funding Acquisition, Y.T.

Funding: This research was funded by the National Natural Science Foundation of China (No. 51702226) and the Natural Science Foundation of Shanxi Province (No. 201701D221078).

Conflicts of Interest: The authors declare no conflict of interest.

References

1. Sasi, B.; Gopchandran, K.G.; Manoj, P.K.; Koshy, P.; Rao, P.P.; Vaidyan, V.K. Preparation of transparent and semiconducting NiO films. *Vacuum* **2002**, *68*, 149–154. [[CrossRef](#)]
2. Liu, H.; Zheng, W.; Yan, X.; Feng, B. Studies on electrochromic properties of nickel oxide thin films prepared by reactive sputtering. *J. Alloy. Compd.* **2008**, *462*, 356–361. [[CrossRef](#)]
3. Mahmoud, S.A.; Akl, A.A.; Kamal, H.; Abdel-Hady, K. Opto-structural, electrical and electrochromic properties of crystalline nickel oxide thin films prepared by spray pyrolysis. *Physica B* **2002**, *311*, 366–375. [[CrossRef](#)]
4. Maruyama, T.; Arai, S. The electrochromic properties of nickel oxide thin films prepared by chemical vapor deposition. *Sol. Energy Mater. Sol. Cells* **1993**, *30*, 257–262. [[CrossRef](#)]
5. Guo, W.; Hui, K.N.; Hui, K.S. High conductivity nickel oxide thin films by a facile sol-gel method. *Mater. Lett.* **2013**, *92*, 291–295. [[CrossRef](#)]
6. Subramanian, B.; Ibrahim, M.M.; Senthilkumar, V.; Murali, K.R.; Vidhya, V.S.; Sanjeeviraja, C.; Jayachandran, M. Optoelectronic and electrochemical properties of nickel oxide (NiO) films deposited by DC reactive magnetron sputtering. *Physica B* **2008**, *403*, 4104–4110. [[CrossRef](#)]
7. Ismail, R.A.; Ghafori, S.A.; Kadhim, G.A. Preparation and characterization of nanostructured nickel oxide thin films by spray pyrolysis. *Appl. Nanosci.* **2013**, *3*, 509–514. [[CrossRef](#)]
8. Jahromi, S.P.; Huang, N.M.; Kamalianfar, A.; Lim, H.N.; Muhamad, M.R.; Yousefi, R. Facile synthesis of porous-structured nickel oxide thin film by pulsed laser deposition. *J. Nanomater.* **2012**, *2012*, 97. [[CrossRef](#)]
9. Soo Kim, D.; Chul Lee, H. Nickel vacancy behavior in the electrical conductance of nonstoichiometric nickel oxide film. *J. Appl. Phys.* **2012**, *112*, 034504. [[CrossRef](#)]
10. Nandy, S.; Saha, B.; Mitra, M.K.; Chattopadhyay, K.K. Effect of oxygen partial pressure on the electrical and optical properties of highly (200) oriented p-type Ni_{1-x}O films by DC sputtering. *J. Mater. Sci. Lett.* **2007**, *42*, 5766–5772. [[CrossRef](#)]
11. Sato, H.; Minami, T.; Takata, S.; Yamada, T. Transparent conducting p-type NiO thin films prepared by magnetron sputtering. *Thin Solid Films* **1993**, *236*, 27–31. [[CrossRef](#)]
12. Nandy, S.; Maiti, U.N.; Ghosh, C.K.; Chattopadhyay, K.K. Enhanced p-type conductivity and band gap narrowing in heavily Al doped NiO thin films deposited by RF magnetron sputtering. *J. Phys.* **2009**, *21*, 115804. [[CrossRef](#)] [[PubMed](#)]
13. Keraudy, J.; Ferrec, A.; Richard-Plouet, M.; Hamon, J.; Goullet, A.; Jouan, P.Y. Nitrogen doping on NiO by reactive magnetron sputtering: A new pathway to dynamically tune the optical and electrical properties. *Appl. Surf. Sci.* **2017**, *409*, 77–84. [[CrossRef](#)]
14. Slack, G.A. Crystallography and domain walls in antiferromagnetic NiO crystals. *J. Appl. Phys.* **1960**, *31*, 1571–1582. [[CrossRef](#)]
15. Roth, W.L. Neutron and optical studies of domains in NiO. *J. Appl. Phys.* **1960**, *31*, 2000–2011. [[CrossRef](#)]
16. Qiu, J.; Chen, Z.; Zhao, T.; Chen, Z.; Chu, W.; Yuan, N.; Ding, J. Electrochromic Properties of NiOx Films Deposited by DC Magnetron Sputtering. *J. Nanosci. Nanotechnol.* **2018**, *18*, 4222–4229. [[CrossRef](#)] [[PubMed](#)]
17. Ramasami, A.K.; Reddy, M.V.; Balakrishna, G.R. Combustion synthesis and characterization of NiO nanoparticles. *Mater. Sci. Semicond. Process.* **2015**, *40*, 194–202. [[CrossRef](#)]
18. Zhu, H.; Dong, H.; Laveille, P.; Saih, Y.; Caps, V.; Basset, J.M. Metal oxides modified NiO catalysts for oxidative dehydrogenation of ethaneto ethylene. *Catal. Today* **2014**, *228*, 58–64. [[CrossRef](#)]

19. Mironova-Ulmane, N.; Kuzmin, A.; Grabis, J.; Sildos, I.; Voronin, V.I.; Berger, I.F.; Kazantsev, V.A. Structural and magnetic properties of nickel oxide nanopowder. *Solid State Phenom.* **2011**, *168*, 341–344. [[CrossRef](#)]
20. Lei, Y.; Li, J.; Wang, Y.; Gu, L.; Chang, Y.; Yuan, H.; Xiao, D. Rapid microwave-assisted green synthesis of 3D hierarchical flower-shaped NiCo₂O₄ microsphere for high-performance supercapacitor. *ACS Appl. Mater. Interfaces* **2014**, *6*, 1773–1780. [[CrossRef](#)]
21. Sasi, B.; Gopchandran, K.G. Nanostructured mesoporous nickel oxide thin films. *Nanotechnology* **2007**, *18*, 115613. [[CrossRef](#)]
22. Asahi, R.; Morikawa, T.; Ohwaki, T.; Aoki, K.; Taga, Y. Visible-light photocatalysis in nitrogen-doped titanium oxides. *Science* **2001**, *293*, 269–271. [[CrossRef](#)] [[PubMed](#)]
23. Wu, K.R.; Hung, C.H. Characterization of N, C-codoped TiO₂ films prepared by reactive DC magnetron sputtering. *Appl. Surf. Sci.* **2009**, *256*, 1595–1603. [[CrossRef](#)]
24. Aduru, S.; Contarini, S.; Rabalais, J.W. Electron-, X-ray-, and ion-stimulated decomposition of nitrate salts. *J. Phys. Chem.* **1986**, *90*, 1683–1688. [[CrossRef](#)]
25. Simon, P.; Pignon, B.; Miao, B.; Coste-Leconte, S.; Leconte, Y.; Marguet, S.; Herlin-Boime, N. N-doped titanium monoxide nanoparticles with TiO rock-salt structure, low energy band gap, and visible light activity. *Chem. Mater.* **2010**, *22*, 3704–3711. [[CrossRef](#)]
26. Duarte, D.A.; Sagás, J.C.; da Silva Sobrinho, A.S.; Massi, M. Modeling the reactive sputter deposition of N-doped TiO₂ for application in dye-sensitized solar cells: Effect of the O₂ flow rate on the substitutional N concentration. *Appl. Surf. Sci.* **2013**, *269*, 55–59. [[CrossRef](#)]
27. Jang, W.L.; Lu, Y.M.; Hwang, W.S.; Chen, W.C. Electrical properties of Li-doped NiO thin films. *J. Eur. Ceram. Soc.* **2010**, *30*, 503–508. [[CrossRef](#)]
28. Zhang, S.; Ali, N. (Eds.) *Nanocomposite Thin Films and Coatings: Processing, Properties and Performances*; Imperial College Press: London, UK, 2007; p. 299.
29. Nguyen, D.T.; Ferrec, A.; Keraudy, J.; Richard-Plouet, M.; Goulet, A.; Cattin, L.; Jouan, P.Y. Ellipsometric and XPS characterization of transparent nickel oxide thin films deposited by reactive HiPIMS. *Surf. Coat. Technol.* **2014**, *250*, 21. [[CrossRef](#)]
30. Ahn, K.S.; Deutsch, T.; Yan, Y.; Jiang, C.S.; Perkins, C.L.; Turner, J.; Al-Jassim, M. Synthesis of band-gap-reduced p-type ZnO films by Cu incorporation. *J. Appl. Phys.* **2007**, *102*, 023517. [[CrossRef](#)]
31. Baumanis, C.; Bahnemann, D.W. TiO₂ thin film electrodes: Correlation between photocatalytic activity and electrochemical properties. *J. Phys. Chem. C* **2008**, *112*, 19097–19101. [[CrossRef](#)]
32. Fogler, H.S. *Elements of Chemical Reaction Engineering*, 2nd ed.; Prentice-Hall: New York, NY, USA, 1992; p. 254.
33. Liu, J.; Huang, X.; Li, Y.; Zhong, Q.; Ren, L. Preparation and photoluminescence of ZnO complex structures with controlled morphology. *Mater. Lett.* **2006**, *60*, 1354–1359. [[CrossRef](#)]
34. Kumari, L.; Li, W.Z.; Vannoy, C.H.; Leblanc, R.M.; Wang, D.Z. Vertically aligned and interconnected nickel oxide nanowalls fabricated by hydrothermal route. *Cryst. Res. Technol.* **2009**, *44*, 495–499. [[CrossRef](#)]
35. Musevi, S.J.; Aslani, A.; Motahari, H.; Salimi, H. Offer a novel method for size appraise of NiO nanoparticles by PL analysis: Synthesis by sonochemical method. *J. Saudi Chem. Soc.* **2016**, *20*, 245–252. [[CrossRef](#)]

